Chip-to-chip optical multimode communication with universal mode processors

Bo Wu[1†], Wenkai Zhang[1†], Hailong Zhou[1*], Jianji Dong[1*] , Dongmei Huang[2,3], P. K. A. Wai[4] and Xinliang Zhang[1]

[†]Bo Wu and Wenkai Zhang contributed equally to this work.

*Correspondence:
hailongzhou@hust.edu.cn;
jjdong@hust.edu.cn

[1] Wuhan National Laboratory for Optoelectronics, School of Optical and Electronic Information, Huazhong University of Science and Technology, Wuhan 430074, China
[2] The Hong Kong Polytechnic University Shenzhen Research Institute, Shenzhen 518057, China
[3] Photonics Research Institute, Department of Electrical Engineering, The Hong Kong Polytechnic University, Hong Kong 999077, China
[4] Department of Physics, Hong Kong Baptist University, Kowloon Tong 999077, Hong Kong, China

Abstract

The increasing amount of data exchange requires higher-capacity optical communication links. Mode division multiplexing (MDM) is considered as a promising technology to support the higher data throughput. In an MDM system, the mode generator and sorter are the backbone. However, most of the current schemes lack the programmability and universality, which makes the MDM link susceptible to the mode crosstalk and environmental disturbances. In this paper, we propose an intelligent multimode optical communication link using universal mode processing (generation and sorting) chips. The mode processor consists of a programmable 4×4 Mach Zehnder interferometer (MZI) network and can be intelligently configured to generate or sort both quasi linearly polarized (LP) modes and orbital angular momentum (OAM) modes in any desired routing state. We experimentally establish a chip-to-chip MDM communication system. The mode basis can be freely switched between four LP modes and four OAM modes. We also demonstrate the multimode optical communication capability at a data rate of 25 Gbit/s. The proposed scheme shows significant advantages in terms of universality, intelligence, programmability and resistance to mode crosstalk, environmental disturbances, and fabrication errors, demonstrating that the MZI-based reconfigurable mode processor chip has great potential in long-distance chip-to-chip multimode optical communication systems.

Keywords: Optical mode generation/sorting, Multimode communication, Optical matrix network, Reconfigurability

Introduction

 The emergence of big data domain is driving the pursuit of higher data transmission rate in a single optical fiber. Different physical dimensions of light, such as wavelength, polarization, and mode, have been exploited to increase the optical communication capacity [1, 2]. Unlike the wavelength and polarization dimensions which have been widely employed in the real optical communication system, the multiplexing of optical modes in multimode fibers is still in the laboratory. Various mode bases such as linearly polarized (LP) modes, orbital angular momentum (OAM) modes and other optical modes in multicore fiber have been extensively studied [3, 4] and their transmission media (multimode fiber, ring-core fiber, and multi-core fiber) have also been developed to support

the long-distance communication [5]. However, the reported chip-to-chip MDM communication links are still in the short-distance domain (less than 10 m) [2, 6], because MDM system is still facing a tough challenge of mode crosstalk, which is ubiquitous in the process of mode generation, transmission, and sorting. Since the traditional mode generator and sorter lack effective programmability [7–14], the long-distance MDM communication links tend to require complex algorithms deployed on electronic digital signal processing (DSP) to compensate the mode crosstalk and environmental disturbances, which largely increases the extra compensating cost.

The Mach-Zehnder interferometer (MZI)-based optical mesh is capable of performing any linear transformation on chip with strong reconfigurability and has been applied to optical matrix computation, optical signal processing, optical polarization/mode processing, etc. [15–21]. It has shown great potential in the optical multiple-input multiple-output (MIMO) descrambler because it can perform the inverse transformation of the crosstalk matrix in the multi-core-fiber-based MDM communication system [22, 23]. Similarly, the MZI mesh is promising to resolve the mode crosstalk in the multimode-fiber-based communication system once the orthogonal fiber modes can be properly generated or sampled on chip.

In this paper, we show theoretically and experimentally that the reconfigurable optical unitary MZI network can act as both a mode generator and a mode sorter in an intelligent MDM communication system. The mode processor is scalable and can be intelligently switched between LP and OAM operation with any routing state and low mode crosstalk. In the experiment, a 25 GHz high-speed intelligent communication is achieved in a chip-to-chip link. Moreover, the mode processor is compatible with other multiplexing technology in a single chip. Overall, our results demonstrate that the proposed architecture is promising to handle complex application scenarios in the long-distance multimode communication.

Results

Principle and chip fabrication

The chip-to-chip multimode communication setup is presented in Fig. 1(a). The basic building block of the mode processor (generator and sorter) is a 4×4 MZI unitary matrix as shown in Fig. 1(b). Each MZI consists of two phase shifters on its inner and outer arms. By adjusting the phase shifters in the network, any 4×4 unitary transmission matrix can be realized (See S1 of Supplementary material). For the mode sorter, there is a 2×2 sampling grating array that can orthogonally sample the LP and OAM modes (Fig. 1(c)). For the LP and OAM modes, the orthogonal sampling matrix can be written as

$$S_{LP} = \frac{1}{2}\begin{pmatrix} 1 & 1 & 1 & 1 \\ 1 & -1 & 1 & -1 \\ 1 & -1 & -1 & 1 \\ 1 & 1 & -1 & -1 \end{pmatrix}, S_{OAM} = \frac{1}{2}\begin{pmatrix} 1 & 1 & 1 & 1 \\ 1 & i & -i & -1 \\ 1 & -1 & -1 & 1 \\ 1 & -i & i & -1 \end{pmatrix}, \tag{1}$$

where the column vectors from left to right represent the complex amplitude of the LP_{01}, LP_{11a}, LP_{11b} and LP_{21} modes (or OAM_0, OAM_1, OAM_{-1} and OAM_2 modes) sampled by the 2×2 sampling grating array, respectively. Then the MZI unitary matrix routes the sampled orthogonal modes to the desired output ports. As an example, the unitary
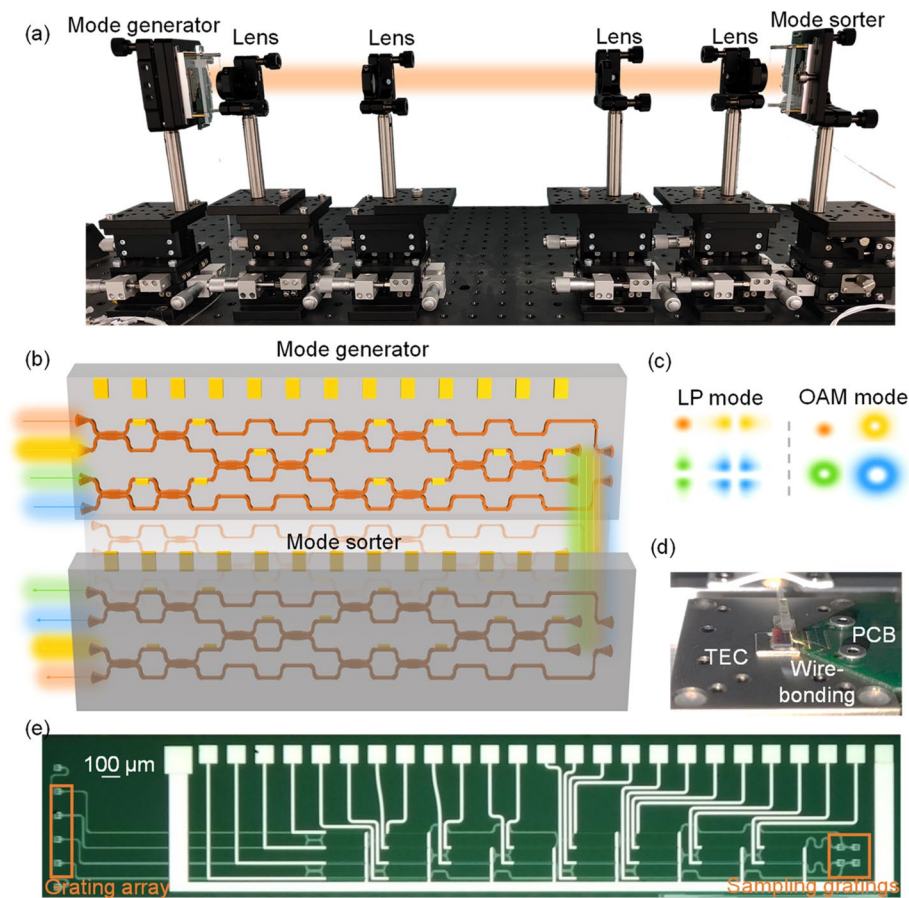
Fig. 1 Working principle and chip fabrication of the intelligent mode processor. **a** The chip-to-chip MDM system setup. **b** The mode processor consists of four aligned single-mode gratings, a 4 × 4 optical MZI unitary matrix and a 2 × 2 grating antenna transmitter/receiver. The mode generator generates orthogonal optical modes (LP modes or OAM modes) through customized training. These modes carry different information and are mixed during transmission. The mode sorter is trained to separate these modes and transmit them to the desired output port. **c** The mode patterns of LP modes and OAM modes. **d** The optical and electrical package of the chip. **e** The microscope image of the fabricated chip

transformation for (Mode1-Port2, Mode2-Port3, Mode3-Port4, Mode4-Port1) can be written as

$$
\begin{pmatrix} 0\ 0\ 0\ 1 \\ 1\ 0\ 0\ 0 \\ 0\ 1\ 0\ 0 \\ 0\ 0\ 1\ 0 \end{pmatrix} = U_{MZI}S_{LP/OAM},
\tag{2}
$$

where U_{MZI} is the transmission matrix of a 4 × 4 MZI mesh. Owing to the orthogonality of the input and output matrices, there is always a unitary matrix U_{MZI} that can satisfy any possible routing. The mode generator can be seen as a reverse processor of the mode sorter. In this case, the 2 × 2 grating array serves as a mode emitting antenna. In S2 of supplementary materials, we compare three types of optical matrices and point out why we choose MZI mesh in this application. Although the generated mode is a sampled version of the original mode, it can only excite the corresponding original mode in the multimode fiber owing to the orthogonality. For ease of discussion, the quasi-LP

and quasi-OAM modes generated by the chip will be referred to simply as LP and OAM modes in the remainder of this paper. By combining the mode generator and the mode sorter, a complete chip-to-chip MDM system can be constructed (Fig. 1(a)). The free space is used to transmit the optical modes, while a multimode fiber can also be used for long-distance communication (See the Discussion section). It is noteworthy that while there is mode crosstalk in the transmission link (With unitary crosstalk matrix *C*), the mode sorter can still be intelligently configured to cancel it:

$$\begin{pmatrix} 0 & 0 & 0 & 1 \\ 1 & 0 & 0 & 0 \\ 0 & 1 & 0 & 0 \\ 0 & 0 & 1 & 0 \end{pmatrix} = U_{MZI}S_{LP/OAM}C. \tag{3}$$

We fabricate the mode processor on a standard 220 nm SOI wafer (Fig. 1(e)). The structure of the MZI mesh follows the topology proposed by Clement et al. [24]. The TiN heaters on the MZI can be electrically tuned to modify the unitary transmission matrix. The size of the 2×2 grating array is 80×80 μm^2. The chip is optically and electrically well packaged except for the 2×2 grating array, which will emit/receive the optical modes to/from the free space (Fig. 1(d)).

Training of the optical mode processor

To train a mode generator, the most efficient method is to train it as a mode sorter because it is easier to generate LP and OAM modes by spatial light modulator (SLM) than to examine them. Figure 2(a) shows the experimental setup for training the mode generator. The output of a 1560-nm continuous wave laser is expanded and collimated from a single-mode optical fiber into the free space by a fiber collimator. The collimated light is then modulated by an SLM, where the phase distribution of LP and OAM modes is loaded. The phase patterns on the SLM and the corresponding far-field distributions of the optical modes generated by the SLM are shown in Fig. 2(b) (See S3 in the Supplementary material for the validation of the OAM modes). After the spatial Fourier transform of a lens with focal length of 50 mm, the diameter of the collimated light will match the size of the 2×2 grating array, thus ensuring a satisfactory coupling efficiency. The chip is controlled by a field programmable gate array (FPGA) module and intelligent algorithm. A lot of algorithms can be employed to train the MZI mesh, like particle swarm optimization, genetic algorithm and gradient decent algorithm (GDA) [25–27]. We adopt GDA here because it will converge faster in a small model. The loss function of the training is defined as

$$L = -\min([ER_1, ER_2, ER_3, ER_4]), ER_k = P_k / (P_{total} - P_k), \tag{4}$$

where P_k and P_{total} are the output power of the desired output port and the total output power of all output ports respectively, when the *k*-th optical mode is input. ER_k represents the extinction ratio of the *k*-th mode. The process of the gradient decent algorithm is as follows.
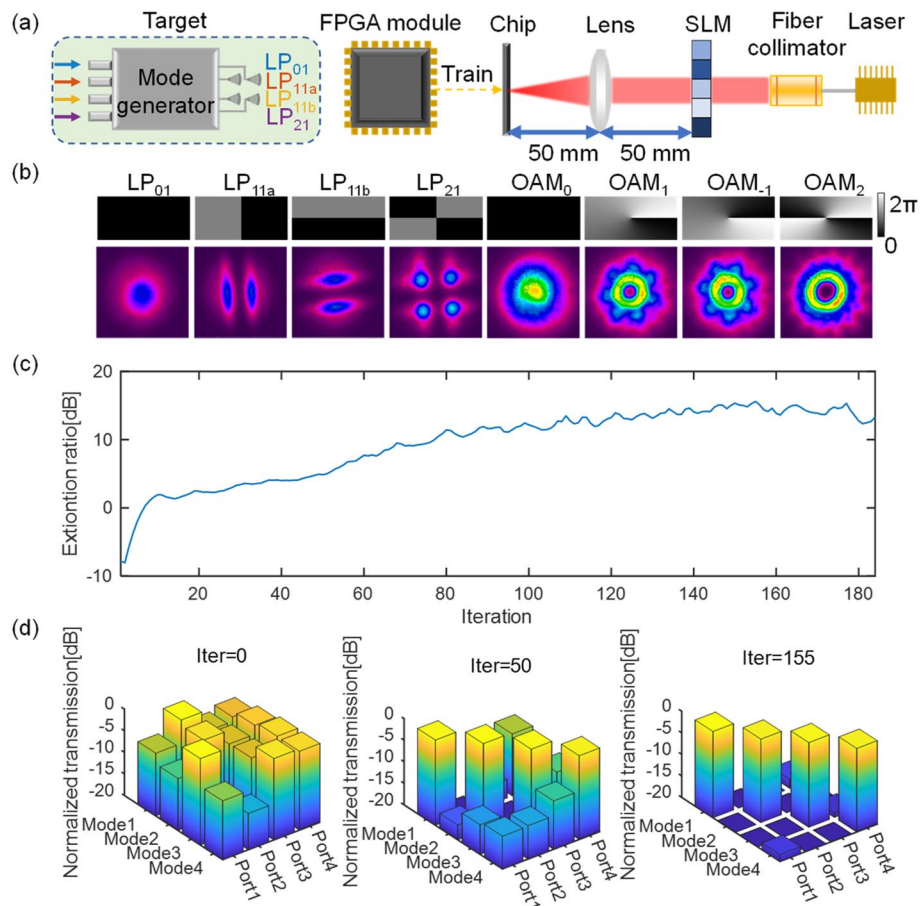
Fig. 2 Training the generator chip. **a** Experimental setup for training the mode generator. The phase distribution of the four LP modes is loaded onto the spatial light modulator (SLM), and a lens is used to match the size of the generated LP modes and the grating antenna array. **b** The far-field distribution of the optical modes generated by the SLM with corresponding phase distribution. **c** The evolution of the lowest extinction ratio among the four LP modes during training. **d** The bar chart of the routing state during training

(A) Randomly initialize the voltages applied to the heaters;

(B) Increase the voltage by 0.01 V for each heater and evaluate the loss function $L(U+0.01)$ respectively;

(C) Decrease the voltage by 0.01 V for each heater and evaluate the loss function $L(U-0.01)$ respectively;

(D) Estimate the gradient of the loss function by.

$$G = \frac{L(U+0.01) - L(U-0.01)}{0.02} \tag{5}$$

(E) Update the voltages using the Adam algorithm, which is a fast-converging gradient decent algorithm [28]
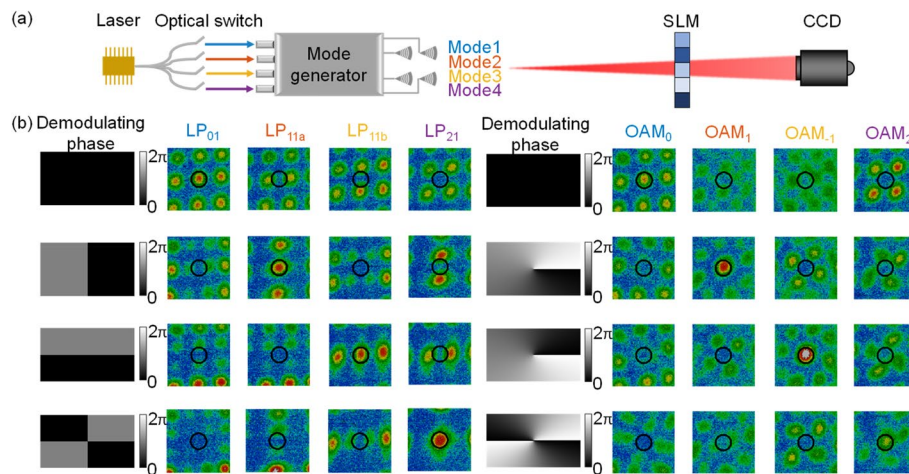
Fig. 3 Verification of chip-generated orthogonal modes. **a** The experimental setup for testing the modes generated by the trained mode generator. The SLM is used to demodulate the four orthogonal modes. A CCD is placed behind the SLM to capture the far-field interference pattern. **b** The far-field interference pattern of the demodulated LP and OAM modes (generated by the mode generator). The interference centers are marked with black circles

$$U(iter + 1) = U(iter) - \alpha(v_{iter}/1 - \beta_1{}^{iter})/\sqrt{s_{iter}/(1 - \beta_2{}^{iter}) + \epsilon},$$
$$v_{iter} = \beta_1 v_{iter-1} + (1 - \beta_1)G, \tag{6}$$
$$s_{iter} = \beta_2 s_{iter-1} + (1 - \beta_2)G^2,$$

where *iter* is the current iteration, α is the learning rate which is set to be 0.05 during training, β_1, β_2 and ε are set to be 0.9, 0.999 and 10^{-8}, respectively. The initial values of v_{iter} and s_{iter} are zero.

(F) Repeat steps (*B-E*) until the loss function converges and the best voltages are stored.

Fig. 2(c) shows the evolution of the minimum *ER* during the training of the mode routing in Fig. 2(a). At training epoch of 155, the minimum *ER* is more than 15 dB. Fig. 2(d) shows three mode transmission matrices at the different stages of training, indicating the effectiveness of the training. Using the method described above, we obtain a set of voltages that can generate four OAM modes. (See S3 in the Supplementary material for more experimental results on the sorting of SLM-generated LP and OAM modes).

Figure 3(a) shows an experimental setup to study the generated modes with the chip. The mode is first demodulated by the SLM and a CCD is placed behind the SLM to capture the far-field interference pattern. When no phase pattern is loaded on the SLM, the far-field pattern will reflect the mode type. As shown in Fig. 3(b), the far-field pattern of the LP modes is a two-dimensional spot array and different modes have different center position offsets. Compared with the LP$_{01}$ mode, the LP$_{11a}$ and LP$_{11b}$ modes have a horizontal and vertical half-period offset, while the LP$_{21}$ mode has a simultaneous horizontal and vertical half-period offset. For the OAM mode, the OAM$_0$ and OAM$_2$ modes have the same pattern as the LP$_{01}$ and LP$_{21}$ modes because their sampled vectors from the 2×2 grating array are

the same. Compared with the LP_{01} mode, the patterns of the OAM_1 and OAM_{-1} modes are rotated by 45 degrees, and become blurred since the phase difference of adjacent spots is $\pm\pi/2$. The experimental results are in good agreement with the simulation (see S4 in the Supplementary material), indicating the successful generation of the designated optical modes. After demodulation by the SLM, the corresponding mode will have a bright spot in the center, while the center of other modes will be dark. In Fig. 3(b), only the diagonal patterns show bright centers, indicating that the generated modes have high purity. It should be noted that although the demodulated OAM_2 mode has a weaker intensity in our experiment, its mode extinction ratio is still very high (Fig. S3 in supplementary material), which is mainly owing to its larger sampling loss and can be compensated with stronger optical input power.

Demonstration of the MDM system

To demonstrate a real application of the intelligent mode processor, we build a chip-to-chip MDM communication system. As shown in Fig. 4(a), the mode generator and sorter are connected by a lens system. The lens, with a short focal length of 25 mm, is used to effectively collimate the dispersed optical mode so that the alignment of the lens system can be easier. After calibrating of the optical path, we can measure the insertion loss of the eight optical modes generated by the mode generator (see Table 1). Considering the loss of the grating coupler and the MZI mesh (about 25 dB), the extra loss in the 4f coupling is $5\sim 8$ dB, which is acceptable in the MDM system. The insertion loss of chip in the system can be further optimized to 9.6 dB with state-of-art technology (See S5 in the Supplementary material for details).

The mode sorter is trained using the same rule as described above. Figure 4(b) and 4(c) show the evolution of the minimum extinction ratio and the three mode transmission matrices at different stages of training. The extinction ratio in the chip-to-chip experiment (18 dB $\sim$ 20 dB) is generally higher than that in the SLM-space-chip experiment (about 15 dB), because the 4f system can more easily satisfy the orthogonality condition of mode sampling. To demonstrate the reconfigurability of our system, three other routing schemes are trained and their final mode transmission matrices are shown in Fig. 4(d), where a mode extinction ratio of more than 18 dB can be achieved. Theoretically, any routing with a high mode extinction ratio can be achieved. (See S6 in the Supplementary material for more experimental results on the performance of the MDM system).

We also test the spectral response of the system. The results are shown in Fig. 5(a) and 5(b) for LP modes and OAM modes, respectively. We can obtain a mode extinction ratio of more than 18 dB at a single wavelength and more than 10 dB at a bandwidth of 10 nm. The bandwidth can be further increased by designing a wavelength-insensitive MZI mesh. To demonstrate its potential in high-speed communications, a 25 Gbit/s pseudorandom binary sequence (PRBS) optical signal is divided equally among the four ports of the mode generator. After training the mode sorter, the undistorted signal is output from the output

Table 1 Insertion loss of the chip-to-chip MDM system

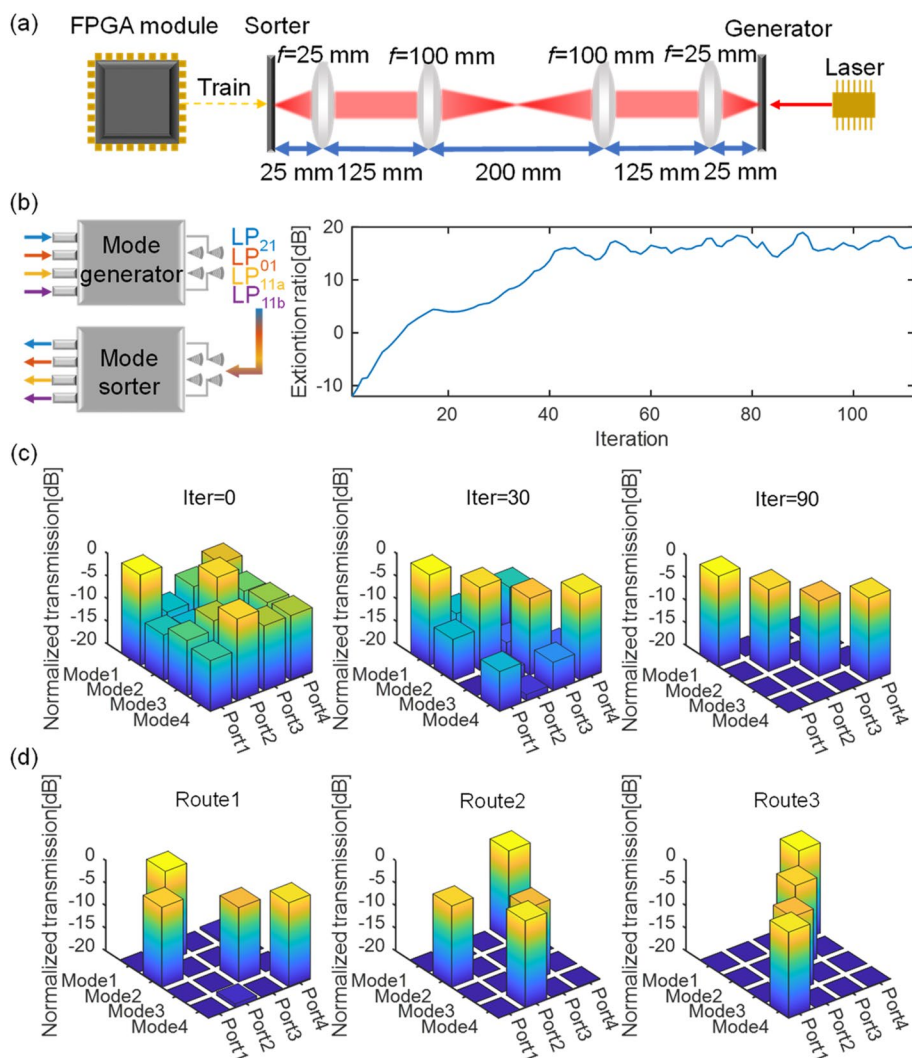| Mode	LP_{21}	LP_{01}	LP_{11a}	LP_{11b}	OAM_0	OAM_1	OAM_{-1}	OAM_2
Insertion loss (dB)	29.79	32.33	32.88	31.61	30.81	32.65	33.08	31.08

Fig. 4 The training of chip-to-chip MDM communication. **a** Experimental setup of the MDM communication system. A 4f system consisting of four lenses perfectly transmits the generated modes to the grating antenna array of the mode sorter. **b** The evolution of the lowest extinction ratio among four chip-generated LP modes during training. **c** The bar chart of the routing state during training. **d** The bar charts of three different routing schemes after their respective training

ports of the mode sorter. On the right side of Fig. 5(a) and 5(b), we show the eye diagrams of the demodulated signals (see S7 in the Supplementary material for the original and the distorted eye diagram). Some degradation of the signal quality (mode2 and mode3 of OAM) is attributed to the imbalance of the insertion loss and the interference of different modes. To demonstrate the crosstalk resistance of the system, we perform another experiment to add an arbitrary disturbance in the mode generator during the training (See S8 of the supplementary material) and we get a recover of the extinction ratio with the help of algorithm. Overall, the demonstration of the chip-to-chip MDM communication verifies the practicality of our proposed scheme.
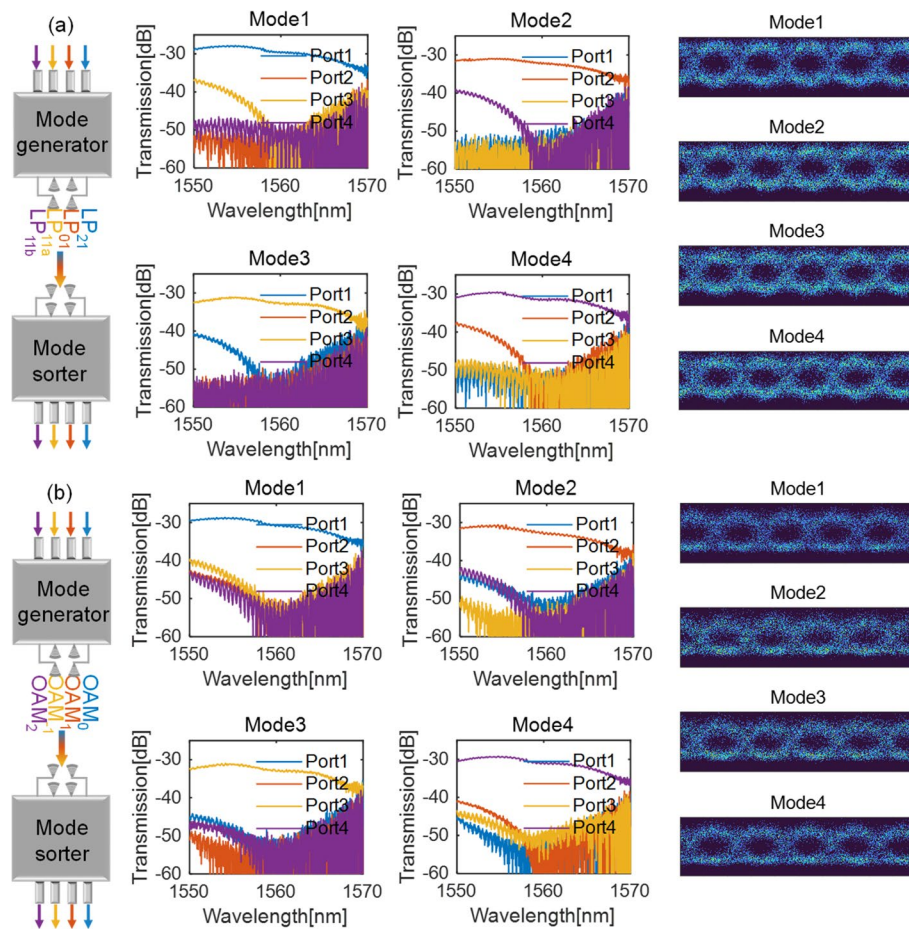
Fig. 5 The optical spectral response and high-speed performance of the proposed optical MDM communication system for (**a**) LP modes and (**b**) OAM modes. The insertion loss includes the loss of the two chips and the loss during the transmission. The eye diagrams are captured with a 25 Gbit/s PRBS optical signal simultaneously incident on the four ports of the mode generator

Discussion

Scalability of the optical mode processor

In this section, we will provide a comprehensive illustration of the scalability of our proposed optical mode processor. In Eq. 1, S_{LP} and S_{OAM} correspond to a Hadamard matrix and a discrete Fourier transform (DFT) matrix, respectively. These two types of matrices are typical unitary matrices. We will now show that evenly spaced circular grating couplers can achieve the orthogonal sampling of the higher-order LP and OAM modes. For an $N \times N$ DFT matrix, the element in the m-th row and the n-th column is $e^{-j2\pi(m-1)(n-1)/N}$. The trajectory of the complex angle of the n-th column vector can be seen to rotate from 0 to 2π for n-1 times, which is consistent with the phase distribution of the OAM_{n-1} modes. Moreover, the OAM_k and OAM_{k-N} ($k > 0$) will have the same sampled phase distribution when there are N grating couplers. Therefore, some higher-order OAM modes can be replaced by the lower order modes to ensure a more reasonable resource allocation. The same grating coupler distribution can also support LP modes. In this case, the sampled matrix becomes a Hadamard matrix. The N grating couplers can support the modes LP_{01}, LP_{11a}, LP_{11b}, LP_{21a}... $LP_{\frac{N}{2}1}$ modes. In Fig. 6, an example of
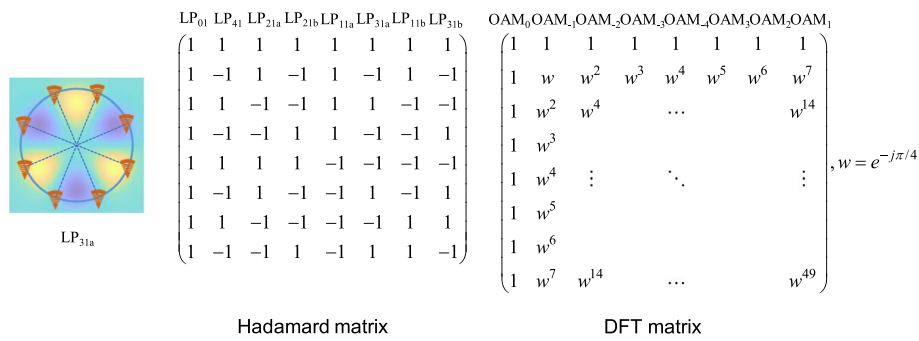
Fig. 6 Orthogonal sampling of LP and OAM modes by eight grating couplers arranged evenly in a circle

$N=8$ is given, and we annotate each orthogonal mode and its sampled vector. For LP modes, the radius of the sampling circle is crucial because the sampled optical intensity should be the same to ensure orthogonality, while for OAM modes it is not an issue due to their circular symmetry. To perform the corresponding unitary transformation, the MZI mesh with the same dimension is necessary. For example, by deploying 8 grating antennas and 8×8 MZI unitary matrix, we can construct the mode processor targeting 8 OAM and LP modes. The scalability of the proposed mode processor makes it very promising for high-capacity communications.

Potential application in long-distance communication

In our experiment, the mode generator and the sorter are connected by free space, which is not an ideal scheme for long-distance communication. Multimode fibers and ring-core fibers are the more competitive transmission media for LP and OAM mode communication because the modes and signals in the fibers are less affected by environmental disturbances. Although there still exists mode crosstalk during the fiber transmission, it can be cancelled by intelligently configuring the mode sorter. When leaving alone the time crosstalk in optical multimode fiber, the transmission distance can be very long because the distance does not change the property of crosstalk as a unitary matrix. As a result, the communication capacity is only restricted by the bandwidth of BPG, modulator and detector. However, with a long transmission distance, the time crosstalk is nonnegligible because of the differential group delay among modes. Once taking time crosstalk into account, the transmission length is limited in the high-speed communication. The time-mode mixing descrambling is necessary in this case [23]. In a multimode communication system that involves amplifiers, the uneven amplification of each mode can be deemed as a diagonal matrix sandwiched between two unitary matrices. Correspondingly, there should be an extra diagonal matrix and unitary matrix on chip to descramble the crosstalk. Another key design issue is to match the mode profile of the fiber and the size of the grating antenna. Currently, our grating coupler has a size of 30×50 μm^2, while the diameter of the commercial multimode fiber is 62.5 μm. Generally, the size of multimode fiber increases with the number of modes, which means a larger size of grating array. To accommodate the modes in the multimode fiber, the current size of grating antenna must be shrunk to ensure a moderate coupling efficiency. To the best of our knowledge, the size of grating antenna can be as small as 3 μm×5 μm

in some ladar system [29, 30]. Specifically, the size of grating antenna should be determined by the balanced coupling efficiency of all modes, which should be optimized with mode field simulation in advance (See S9 of supplementary material for the optimization analysis of grating array). In addition, the size of the ring-core fiber should also be carefully designed to match the grating array so that the LP and OAM modes can be randomly switched with the same optical mode generator/sorter. Overall, the proposed architecture is promising for future long-hual fiber communication systems.

Monolithic integrated silicon photonic multi-dimensional transceiver

The proposed mode processor has great potential to be monolithically integrated with other multiplexing technology, i.e., WDM (wavelength division multiplexing) and PDM (polarization division multiplexing). Figure 7 shows a conceptual diagram of the monolithic integrated silicon photonic multi-dimensional transceiver, where the Mach Zehnder modulator (MZM), arrayed waveguide grating (AWG), polarization beam splitter (PBS) and photodetector (PD) can all be integrated with the mode processor on the same silicon chip. There are just a few more considerations: (I) The MZI unitary matrix can be designed to have a large bandwidth but is very hard to be polarization-insensitive because the single mode silicon waveguide has a large birefringence. Therefore, it is more practical to duplicate the mode processor and separate the processing of two polarizations, as shown in Fig. 7. The two TE polarizations are then combined with the polarization splitter rotator (PSR). (II) The grating coupler antenna should also be specifically designed to be polarization-insensitive, either by specific optimization of one-dimensional grating coupler [32] or two dimensional grating coupler. With the state-of-art technology, we can adopt two polarizations, 32 wavelengths with 100 GHz frequency space in the C band, 8 LP/OAM modes and 25 Gbaud 32QAM modulation format [33, 34]. In this case, the communication capacity can reach 64 Tbit/s in a single optical fiber.
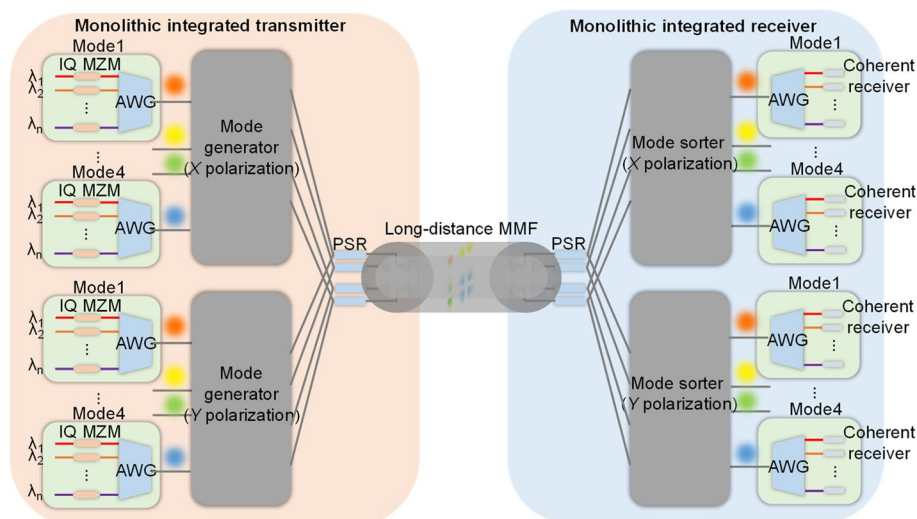

Fig. 7 The conceptual diagram of monolithic integrated silicon photonic multi-dimensional transceiver. MZM, Mach Zehnder modulator. AWG, arrayed waveguide grating. PSR, polarization splitter rotator. MMF, multimode fiber

Conclusions

In conclusion, we have proposed and demonstrated an intelligent optical MDM system based on the reconfigurable MZI unitary matrix. Theoretically, we showed that the optical mode processor can handle both the LP and OAM modes and support any desired routing scheme. Experimentally, we verified the intelligence of the mode processor and carried out a 25 GHz chip-to-chip communication experiment, demonstrating the capability of multimode communication with our mode processor. Furthermore, we have demonstrated its scalability, potential applications in long-distance communication and compatibility with other multiplexing technologies. It shows significant advantages in universality, intelligence, programmability and resistance to disturbances and fabrication errors. Our work paves the way for future intelligent optical MDM communications.

Methods

Details of the experiment

To train the mode generator, the 1560-nm CW laser is first amplified to 23 dBm by an EDFA. After propagating through the SLM (Holoeye HED-6001), the 50 mm focal length lens, and the mode sorter, the optical power output from the chip is measured by a photodetector array electrically connected to the analog-to-digital converter (AD7606). The voltage applied to the heater is provided by the digital-to-analog converter (LTC2688). Both the AD7606 and the LTC2688 are controlled by a field programmable gate array chip (7K325T). The entire experimental system was controlled by a personal computer through serial ports. The mode generator and mode sorter are thermally stabilized by a thermoelectric cooler (TEC). We use the amplified spontaneous emission from the EDFA as the input source, and an optical spectrum analyzer (Yokokawa AQ6319) captures the spectrum of the input source and the output from the chip. The difference between the two measurements is taken as the transmission spectrum of the system. In the high-speed communication experiment, the 1560-nm CW laser is first injected into an optical modulator and modulated by the 25G PRBS code generated by a bit pattern generator (BPG). The modulated optical signal is amplified and split by a 1×4 power splitter. The four channels operate simultaneously and the oscilloscope records the eye diagrams of the signals received by a photodetector (Finisar).

The characterization of fabricated chip

The fabricated grating coupler has a diffraction angle of 12°. Therefore, the two chips are titled in the chip-to-chip communication experiment to ensure optical alignment. At the working wavelength of 1560 nm, the insertion loss of a single grating coupler is about 5 dB. The insertion loss of the 4×4 MZI unitary matrix is about 2.5 dB, which is mainly due to the loss of the 2×2 multimode interferometer (MMI). The total chip loss is about 12.5 dB. The π phase shift power consumption of a single MZI is about 18.4 mW.

Supplementary Information

The online version contains supplementary material available at https://doi.org/10.1186/s43074-023-00114-3.

Additional file 1.

Declarations

Ethics approval and consent to participate
There is no ethics issue for this paper.

Consent for publication
All authors agreed to publish this paper.

Competing interests
The authors declare that they have no competing interests.

References
1. Zhou H, et al. Dielectric metasurfaces enabled ultradensely integrated multidimensional optical system. Laser Photonics Rev. 2022. https://doi.org/10.1002/lpor.202100521.
2. Yang KY, et al. Nat Commun. 2022;13:7862.
3. Zhou HL, Fu DZ, Dong JJ, Zhang P, Chen DX, Cai XL, Li FL, Zhang XL. Light Sci Appl. 2017;6:e16251.
4. Richardson DJ, Fini JM, Nelson LE. Space-division multiplexing in optical fibres. Nat Photonics. 2013;7(5):354–62. https://doi.org/10.1038/nphoton.2013.94.
5. Liu J, et al. 1-Pbps orbital angular momentum fibre-optic transmission. Light Sci Appl. 2022;11(1):202. https://doi.org/10.1038/s41377-022-00889-3.
6. Baumann JM, et al. Silicon chip-to-chip mode-division multiplexing. In: 2018 Optical Fiber Communications Conference and Exposition (OFC), 11-15 March 2018; 2018. p. 1–3.
7. Doerr CR, Fontaine N, Hirano M, Sasaki T, Buhl L, Winzer P. Silicon photonic integrated circuit for coupling to a ring-core multimode fiber for space-division multiplexing. In: European Conference and Exposition on Optical Communications: Optical Society of America; 2011. p. Th. 13. A. 3.
8. Schulz SA, Machula T, Upham J, Karimi E. Boyd RW. In: Chang HTVKT, Watts M, editors. Advanced Photonics 2013. Puerto Rico: (Optica Publishing Group, Rio Grande; 2013. p. IT5A.2.
9. Ding YH, Ou HY, Xu J, Peucheret C. Silicon photonic integrated circuit mode multiplexer. IEEE Photon Technol Lett. 2013;25(7):648–51. https://doi.org/10.1109/Lpt.2013.2247394.
10. Koonen AMJ, Chen HS, van den Boom HPA, Raz O. IEEE Photonics Technol Lett. 2012;24:1961.
11. Liu J, et al. Light. Sci Appl. 2018;7:17148.
12. Xie Z, et al. Light. Sci Appl. 2018;7:18001.
13. Miller DAB. Analyzing and generating multimode optical fields using self-configuring networks. Optica. 2020;7(7). https://doi.org/10.1364/optica.391592.
14. Zhang D, Feng X, Huang Y. Encoding and decoding of orbital angular momentum for wireless optical interconnects on chip. Opt Express. 2012;20(24):26986–95. https://doi.org/10.1364/OE.20.026986.
15. Zhou H, et al. Photonic matrix multiplication lights up photonic accelerator and beyond. Light Sci Appl. 2022;11(1):30. https://doi.org/10.1038/s41377-022-00717-8.
16. Zhou HL, Zhao YH, Wang X, Gao DS, Dong JJ, Zhang XL. Self-Configuring and reconfigurable silicon photonic signal processor. ACS Photonics. 2020;7(3):792–9. https://doi.org/10.1021/acsphotonics.9b01673.
17. Zhou HL, et al. Chip-scale optical matrix computation for PageRank Algorithm. IEEE J Sel Top Quantum Electron. 2020;26(2):1–10. https://doi.org/10.1109/Jstqe.2019.2943347.
18. Zhou HL, Zhao YH, Wei YX, Li F, Dong JJ, Zhang XL. All-in-one silicon photonic polarization processor. Nanophotonics. 2019;8(12):2257–67. https://doi.org/10.1515/nanoph-2019-0310.

19. Shen Y, et al. Deep learning with coherent nanophotonic circuits. Nat Photonics. 2017;11(7):441–6. https://doi.org/10.1038/nphoton.2017.93.

20. Xu X, et al. Self-calibrating programmable photonic integrated circuits. Nat Photonics. 2022. https://doi.org/10.1038/s41566-022-01020-z.

21. Milanizadeh M, et al. Separating arbitrary free-space beams with an integrated photonic processor. Light Sci Appl. 2022;11(1):197. https://doi.org/10.1038/s41377-022-00884-8.

22. Annoni A, Guglielmi E, Carminati M, Ferrari G, Sampietro M, Miller DA, Melloni A, Morichetti F. Light Sci Appl. 2017;6:e17110.

23. Zhang W, et al. On-chip photonic spatial-temporal descrambler. Chip. 2023;2(2). https://doi.org/10.1016/j.chip.2023.100043.

24. Clements WR, Humphreys PC, Metcalf BJ, Kolthammer WS, Walmsley IA. Optimal design for universal multiport interferometers. Optica. 2016;3(12):1460–5. https://doi.org/10.1364/Optica.3.001460.

25. Shao R, Zhang G, Gong X. Generalized robust training scheme using genetic algorithm for optical neural networks with imprecise components. Photonics Res. 2022;10(8):1868–76. https://doi.org/10.1364/Prj.449570.

26. Cong G, et al. On-chip bacterial foraging training in silicon photonic circuits for projection-enabled nonlinear classification. Nat Commun. 2022;13(1):3261. https://doi.org/10.1038/s41467-022-30906-3.

27. Pai S, et al. Experimentally realized in situ backpropagation for deep learning in photonic neural networks. Science. 2023;380(6643):398–404. https://doi.org/10.1126/science.ade8450.

28. Kingma DP, Ba J. Adam: a method for Stochastic optimization. p. arXiv:1412.6980. https://doi.org/10.48550/arXiv.1412.6980.

29. Hu G, Zhong K, Qin Y, Tsang HK. Silicon photonic integrated circuit for high-resolution multimode fiber imaging system. APL Photonics. 2023;8(4). https://doi.org/10.1063/5.0137688.

30. Fatemi R, Khachaturian A, Hajimiri A. IEEE J Solid-State Circuits. 2019;54:1200.

31. Wang X, et al. Polarization-independent fiber-chip grating couplers optimized by the adaptive genetic algorithm. Opt Lett. 2021;46(2):314–7. https://doi.org/10.1364/OL.413307.

32. Xie C, Zou X, Zou F, Yan L, Pan W, Zhang Y. A 32-channel 100 GHz wavelength division multiplexer by interleaving two silicon arrayed waveguide gratings*. Chin Phys B. 2021;30(12):120703. https://doi.org/10.1088/1674-1056/ac2d23.

33. Zhou J, Wang J, Zhang Q. Silicon Photonics for 100Gbaud. In: Optical Fiber Communication Conference (OFC) 2020. San Diego: Optica Publishing Group, in OSA Technical Digest; 2020. p. T3H.4. https://doi.org/10.1364/OFC.2020.T3H.4. Available: https://opg.optica.org/abstract.cfm?URI=OFC-2020-T3H.4.

34. Zhou J, Wang J. Zhang Q. In: Optical Fiber Communication Conference (OFC) 2020. San Diego, California: (Optica Publishing Group; 2020. p. T3H.4.

Publisher's Note

Springer Nature remains neutral with regard to jurisdictional claims in published maps and institutional affiliations.